

Comparison of the SFI Peculiar Velocities with the IRAS 1.2 Jy Gravity Field

Luiz N. da Costa¹, Adi Nusser², Wolfram Freudling³, Riccardo Giovanelli⁴,
Martha P. Haynes⁴, John J. Salzer⁵ and Gary Wegner⁶

¹*European Southern Observatory, Karl-Schwarzschild Str. 2, D-85748 Garching b. München, Germany*

²*Max-Planck-Institut für Astrophysik, Karl-Schwarzschild-Str. 1, D-85749 Garching b. München, Germany*

³*Space Telescope–European Coordinating Facility, European Southern Observatory, Karl-Schwarzschild-Str. 2, D-85748 Garching b. München, Germany*

⁴*Center for Radiophysics and Space Research and National Astronomy and Ionosphere Center, Cornell University, Ithaca, NY 14953*

⁵*Dept. of Astronomy, Wesleyan University, Middletown, CT 06457*

⁶*Dept. of Physics and Astronomy, Dartmouth College, Hanover, NH 03755*

17 September 2018

ABSTRACT

We present a comparison between the peculiar velocity fields measured from the SFI all-sky Sbc-Sc Tully-Fisher catalog and that derived from the *IRAS* 1.2 Jy redshift survey galaxy distribution. The analysis is based on the expansion of these data in redshift space using smooth orthonormal functions and is performed using low and high resolution expansions, with an effective smoothing scale which increases almost linearly with redshift. The effective smoothing scales at 3000 km s⁻¹ are 1500 km s⁻¹ and 1000 km s⁻¹ for the low and high resolution filters. The agreement between the high and low resolution SFI velocity maps is excellent. The general features in the filtered SFI and *IRAS* velocity fields agree remarkably well within 6000 km s⁻¹. This good agreement between the fields allows us to determine the parameter $\beta = \Omega^{0.6}/b$, where Ω is the cosmological density parameter and b is the linear biasing factor. From a likelihood analysis on the SFI and *IRAS* modes we find that $\beta = 0.6 \pm 0.1$ independently of the resolution of the modal expansion. For this value of β , the residual fields for the two filters show no systematic variations within 6000 km s⁻¹. Most remarkable is the lack of any coherent, redshift dependent dipole flow in the residual field.

Key words: cosmology: observations – dark matter – large scale structure of Universe

1 INTRODUCTION

Measurements of the peculiar motions of galaxies in the nearby universe represent one of the most powerful tools currently available to probe mass fluctuations on large scales ($\lesssim 100h^{-1}Mpc$). Furthermore, in conjunction with redshift surveys, the relationship between the distribution of luminous and dark matter can be investigated. Peculiar motions also offer an alternative estimate of the cosmological density parameter Ω on intermediate scales, complementing other dynamical measures on smaller scales (Fisher et al. 1994, Carlberg et al. 1996), and global determinations such as the magnitude-redshift diagram of SN Ia (*e.g.*, Perlmutter et al. 1997) and statistics of gravitational lenses (Kochanek 1996). Estimates of Ω from peculiar motions can be derived either using general assumptions about the initial fluctuations (*e.g.*, Nusser & Dekel 1993) that are independent of the galaxy distribution, or by combining the peculiar velocity data with redshift surveys (*e.g.* Dekel et al. 1993, Davis, Nusser & Willick 1996, Freudling et al. 1997). The latter case requires an assumption about the biasing relation between the galaxy and the dark matter distribution, which is usually taken to be linear, and leads to an estimate of the parameter $\beta = \Omega^{0.6}/b$ where b is the biasing factor.

Work on this subject has led to some puzzling results. Primarily this is because most earlier work was based in a relatively sparse and inhomogeneous set of galaxies with measured peculiar velocities. Recently, the observational situation has dramatically improved with the completion of large redshift-distance samples in both hemispheres. The most notable are the Mathewson, Ford & Buchhorn survey (1992, MFB92) with about 1200 galaxies with I-band photometry and measured

rotational velocities, either from radio observations of 21-cm linewidths or optical rotation curves, and the I-band Tully-Fisher (TF) distance survey of about 2000 spiral galaxies in the field (SFI survey, da Costa et al. 1996, Haynes et al. 1997) and in the direction of 24 clusters (SCI survey, Giovanelli et al. 1997a). These TF surveys have been used to construct two largely independent all-sky redshift-distance catalogs: the Mark III catalog, which is a compilation of all available data to date (*e.g.*, Willick et al. 1997); the SFI catalog (*e.g.*, da Costa et al. 1996, Haynes et al. 1997) which combines a pruned version of the MFB92 data, south of $\delta = -45^\circ$, with the SFI survey (*e.g.*, da Costa et al. 1996, Haynes et al. 1997).

The SFI catalog has recently been used by da Costa et al. (1996) to reconstruct the mass density and three-dimensional velocity fields. Significant differences were found relative to earlier reconstructions. In particular, for the first time the measured velocity field showed a bifurcation with some galaxies flowing towards the Great Attractor (GA) while others moving towards the Perseus-Pisces complex (PP), a feature seen in the *IRAS* velocity field. In that paper it was conjectured that the better agreement between the gross features of the flows was likely to have an impact on the accuracy with which the parameter β could be determined since it relies on a good match between the observed and predicted velocity fields.

The main goals of the present paper are: 1) to investigate more quantitatively the agreement between the measured radial peculiar velocities and the *IRAS* predicted gravity field; 2) to use the velocity-velocity comparison to determine the parameter β ; 3) to compare the results with those obtained from a similar analysis of the Mark III catalog.

The current analysis uses the the method of orthogonal mode-expansion (ITF method) developed by Nusser & Davis (1995, ND95). The main advantages of the method are that it uses the inverse TF relation, which as shown by Schechter (1980) reduces the effects of Malmquist bias, requires no binning of the data and provides a smooth map of the velocity field. The method is ideal for comparing different datasets and provides a useful way of displaying the velocity field. Furthermore, since it has recently been applied to the Mark III catalog by Davis, Nusser & Willick (1996, DNW) we can indirectly compare these two catalogs. Understanding the differences between these catalogs is important for this may make it possible to combine all the currently available samples.

In section 2, we briefly describe the SFI redshift-distance catalog. In section 3, we review the basics of the ITF method and describe our choice of basis function. In section 4, we apply the method to the SFI catalog and present low and high resolution maps for the SFI radial velocity field and compare them to the predicted *IRAS* gravity field for different assumed values of β . The likelihood method used to derive β is discussed in section 4. A brief summary of our conclusions is presented in section 5.

2 DATA

The TF data used here consists of two sets: the first is the SFI survey, an I-band and 21 cm survey of Sbc-Sc galaxies with inclinations $\gtrsim 45^\circ$, north of $\delta \geq -45^\circ$ and galactic latitudes $b > 10^\circ$. Galaxies were drawn according to the following redshift-dependent criteria: $2.5' < a < 5' \quad cz < 3000 \text{ km s}^{-1}$; $1.6' < a < 5' \quad 3000 < cz < 5000 \text{ km s}^{-1}$; $1.3' < a < 5' \quad 5000 < cz < 7500 \text{ km s}^{-1}$. The second is a pruned version of the MFB92 survey, including only Sbc-Sc galaxies. The original MFB92 measurements of magnitude and rotational velocities, either from 21 cm line widths or optical rotation curves, were converted into the SFI system using galaxies in common with the SFI survey. For the MFB92 galaxies with only optically measured line widths, we have used the kinematically centered rotation curves of Persic & Salucci (1995) to derive the rotational velocities at one optical radius in order to bring them on a common scale. These values were used to calibrate the relation between the MFB92 rotational velocities and our 21 cm line widths. We also use the overlapping set of galaxies to transform the MFB92 magnitudes into the SFI system (Giovanelli et al. 1997a).

3 METHOD

In linear theory, the velocity field is related to gravity by the parameter $\beta = \Omega^{0.6}/b$. Our aim is to estimate of the underlying peculiar velocity field from the SFI data and compare it with the velocity field predicted from the gravity field computed from the *IRAS* galaxy redshift distribution.

In order to derive a smooth velocity field from the SFI data we use the method developed by ND95, based on the inverse TF relation. We assume that the rotational velocity parameter $\eta = \log(W) - 2.5$, where W is the line width, is related to its absolute magnitude M by means of a linear inverse TF relation

$$\eta = \gamma M + \eta_0, \quad (1)$$

where γ and η_0 are, respectively, the slope and the zero point of the relation.

The method is designed to describe the underlying velocity field by a set of smooth functions. Following ND95 we write $M_i = M_{0i} + P_i$, where $M_{0i} = m - 5 \log(s_i) - 15$, $P_i = 5 - \log(1 - u_i/s_i)$, m_i is the apparent magnitude of the galaxy, $s_i = cz_i$ is its redshift in km s^{-1} and u_i its radial peculiar velocity. The method assumes that the function P can be expanded in a set of smooth functions, *i.e.*, .

$$P_i = \sum \alpha^j F_i^j, \quad (2)$$

where the functions F_i^j are orthonormal in the space of the data points, *i.e.*, $\sum_i F_i^j F_i^{j'} = \delta_{K}^{jj'}$.

The coefficients α^j and the ITF parameters, γ and η_0 , are then found simultaneously by minimizing

$$\chi^2 = \sum \frac{[\eta_0 + \gamma(M_{0i} + \sum_j \alpha^j F_i^j) - \eta_i]^2}{\sigma_\eta^2}, \quad (3)$$

where σ_η is the rms scatter of the inverse relation.

We choose the zeroth mode to describe a Hubble flow in the space of the data set, *i.e.*, $F_i^0 = 1/\sqrt{N_g}$ where N_g is the number of galaxies in the sample. Therefore the mode α^0 fixes the zero point of the ITF relation. Here we arbitrarily set $\alpha^0 = 0$ in the following analysis. In the comparison between the *IRAS* and ITF fields we subsequently remove such a Hubble flow from the *IRAS* velocity field. Thanks to the uniformity of the SFI sample, this correction is negligible. Following DNW we construct the higher order functions F_j from spherical harmonics Y_l^m for the angular wavefunctions (Fisher et al. 1995) and derivatives of spherical Bessel functions, $j_l[y(z)]$ for the radial basis functions, where the transformation from z to y in the argument of these Bessel functions is designed to make them oscillate non-uniformly with depth in order to match the spatial distribution of the TF data. The use of the coordinate y instead of z significantly reduces the number of parameters necessary to fit the underlying velocity field in terms of our velocity model (DNW). For the reasons given in DNW, we formulate our model to describe the velocity field with respect to the motion of the Local Group. The velocity model can be written in the form

$$P(s, \theta, \phi) = \sum_{n=0}^{n_{max}} \sum_{l=0}^{l_{max}} \sum_{m=-l}^{m=l} \frac{a_{nlm}}{s} [j'_l(k_n y(s)) - c_{l1}] Y_{lm}(\theta, \phi) \quad . \quad (4)$$

The constant c_{l1} is non-zero only for the dipole term and is introduced to ensure that $P = 0$ at the origin since we work in the LG frame. ND95 give details of the derivation of the orthonormal functions F_i^j . For the SFI data, we find that the following transformation:

$$y = \frac{s}{1000} \left[1 + \left(\frac{s}{1000} \right)^2 \right]^{-1/2}, \quad (5)$$

yields a better fit than $y = s$. For instance, for an assumed value of $\sigma_\eta = 0.065$ (see discussion below), when the flow of 1114 SFI galaxies within 6000 km s^{-1} was fitted with 40 modes, the χ^2 was reduced from 1292 to 1074 with the transformation (5) and to 1092 with $y = s$.

4 ANALYSIS OF THE SFI AND IRAS VELOCITY FIELDS

We apply the above method to the 1114 galaxies within a redshift of 6000 km s^{-1} in the SFI sample. We will present results for low and high resolution smoothings which we label LR and HR, respectively. The LR smoothing corresponds to $l_{max} = 3, n_{max} = 3$ which requires 40 modes while the HR smoothing is obtained from expanding the peculiar velocity fields with 74 modes corresponding to $l_{max} = 4, n_{max} = 4$. In figure 1 we show the variation of the radial resolution as a function of the redshift for the two filters.

The inverse TF parameters we obtain after the modal expansion are, $(\gamma, \eta_0 = -0.117, -2.47)$ and $(\gamma, \eta_0 = -0.118, -2.47)$ for the LR and HR filters, respectively. For $\sigma_\eta = 0.0656$ the χ^2 of the ITF regression of observed versus predicted line-widths drops from 1292 to 1074 and 1050 for LR and HR, respectively. In the following analysis we work with a value of $\sigma_\eta = 0.065$. This value yields a reduced χ^2 equal to unity for the LR filter and very close to unity for the HR filter. Note that a significantly smaller value ($\sigma_\eta = 0.046$), is obtained from the SCI galaxy cluster (Giovanelli et al. 1997b) sample. However, a direct comparison between the field and cluster samples is not trivial. For instance, one possible reason for this difference could be that spirals in clusters form a more homogenous population than those in the field. Note, however, that although the scatter differs significantly, the slopes of inverse TF relation for the SFI and SCI differ only by 4%. In our analysis we do not take into account any possible dependence of the scatter on the absolute magnitudes. In fact, after fitting our velocity model to the SFI data, we did not find any evidence for magnitude dependent η scatter. We point out however that the scatter is not strictly Gaussian.

In order to inspect the performance of the modal expansion, in more detail, in figure 2 we plot the correlation functions of the residuals, $\Delta\eta_i = \eta_i - \gamma M_{0i} - \eta_0$, before and after the modal expansion. For both the LR and HR smoothings, the amplitude of the correlation functions is consistent with zero even on separations smaller than the resolution limit. This plot demonstrates that our procedure successfully extracted the signal from the TF data.

Given an assumed value for β we apply the method of Nusser & Davis (1994) to generate maps of velocity fields from the distribution of the *IRAS* galaxies in space. This method generates velocity fields non-iteratively in redshift space. As input to

this method a density field is provided by smoothing the *IRAS* galaxy distribution with a gaussian window of width equal to half the mean particle separation at a given redshift. Because of our choice of the zeroth point for the ITF relation, we subtract from the *IRAS* velocity fields, any Hubble flow like component at the position of the SFI galaxies. The *IRAS* fields are then expanded in the same orthogonal set of basis functions as employed for the SFI velocities. The *IRAS* and SFI velocities are guaranteed to have the same resolution because the original smoothing of the *IRAS* density field is small compared to the resolution of the modal expansion,

4.1 Smooth Velocity Maps

The resulting LR and HR fits to the measured SFI velocity field are shown in figures 3 and 4, in redshift shells 2000km s^{-1} thick. The infall to Virgo ($l = 284^\circ, b = 74^\circ$) dominates the nearby SFI flow. Other features like Ursa Major and Fornax are poorly sampled by the SFI. In the middle panel, the field exhibits a dipole pattern corresponding to the reflex motion of the Local Group with infalling galaxies in the Hydra-Centaurus direction and an outward flow in the Perseus-Pisces direction, as seen in the LG restframe, which is even stronger in the most distant shell. Comparison of figures 3 and 4 show that despite some small amplitude variations the LR and HR fits are remarkably similar over the entire volume. The good agreement between the two fits is a consequence of the uniform sampling of SFI data. Our ability to fit a higher resolution function also indicates that the solution is stable and insensitive to the smoothing scale.

For comparison, we show in figure 5 the LR *IRAS* field reconstructed with $\beta = 1$. Comparing figures 3 and 5 one immediately sees that although the amplitude of the *IRAS* field with $\beta = 1$ clearly does not match that of the SFI field, the general pattern of the velocity fields is remarkably similar with excellent agreement in the locations of outflows and inflows. This result builds confidence in the possibility of determining an accurate value of β from the velocity-velocity comparison using the observed SFI and predicted *IRAS* fields. To illustrate this, figure 6 shows the *IRAS* flow with $\beta = 0.6$ which clearly yields a much better match to the amplitude of the SFI flow than that obtained with $\beta = 1$. The quality of the match can be evaluated in figures 7 and 8, plotting the residuals from the comparison of the SFI and *IRAS* fields, with $\beta = 0.6$ for the LR and HR fits, respectively. The overall agreement is remarkable with only a few nearby galaxies giving large residuals. Most encouraging is the absence of large regions of coherent residuals and the absence of systematic residuals such as the dipole residual seen in previous analysis at intermediate and distant redshift shells (DNW). Moreover, the amplitude of the residuals is close to that obtained by DNW in the analysis of mock catalogs.

4.2 Determination of β

The filtered SFI and *IRAS* velocity fields are fully described by the modal expansion coefficients, α_{tf}^j and α_{IRAS}^j . Since the number of these coefficients is significantly smaller than the number of galaxies, it is more efficient to estimate β by comparing the modes rather than the velocities of galaxies. Following DNW, we define our best estimate for β as the value which renders a minimum in the Pseudo χ^2

$$\tilde{\chi}^2(\beta) = \sum_{j,j'} [\alpha_{tf}^j - \alpha_{iras}^j(\beta)] [\mathbf{T} + \mathbf{M}(\beta)]^{-1} [\alpha_{tf}^{j'} - \alpha_{iras}^{j'}(\beta)], \quad (6)$$

where $\mathbf{T} \equiv \langle \delta\alpha_{tf}^j \delta\alpha_{tf}^{j'} \rangle$ and $\mathbf{M} \equiv \langle \delta\alpha_{iras}^j \delta\alpha_{iras}^{j'} \rangle$ are the the error covariance matrices of the coefficients α_{tf}^j and α_{iras}^j respectively. The ITF error matrix \mathbf{T} is easy to evaluate, thanks to the orthonormality condition. This matrix is diagonal and is given by

$$T^{jj'} = \left(\frac{\sigma_\eta}{\gamma} \right)^2 \delta_{jj'}^K. \quad (7)$$

The *IRAS* error covariance matrix is more cumbersome to compute. It should incorporate three sources of errors in the *IRAS* velocity field: (i) the peculiar velocities are generated using galaxy redshifts relative to LG frame. Any error in the LG motion creates a dipole discrepancy between the SFI and the *IRAS* velocities. (ii) the *IRAS* density field is estimated from a discrete distribution of galaxies and therefore suffers from Poisson error which propagates into the velocity field. (iii) small scale coherent (as in triple valued zones) nonlinear velocities are not included in the *IRAS* recovered velocities and can be important in the error budget. Note that, in contrast to DNW, we have not included uncertainties due to small scale incoherent (local velocity dispersion) velocities. That is justified because the SFI modes suffer from a similar error which roughly equals the error in the *IRAS* modes. Moreover, since our estimated value for σ_η includes scatter due to incoherent velocities of galaxies in the SFI sample, a somewhat lower value for σ_η than estimated above should be used in evaluating $\tilde{\chi}^2$. Below we will estimate β for various values of σ_η .

We can express the *IRAS* velocity covariance as the sum of these errors

$$\langle \Delta u_i \Delta u_j \rangle = C_{LG}(i, j) + C_{SN}(i, j) + C_{NL}(i, j). \quad (8)$$

where the terms C_{LG} , C_{SN} and C_{NL} depend on β and describe uncertainties due to LG motion, shot-noise and nonlinearities, respectively. The modes covariance matrix, \mathbf{M} , is then computed by projecting the elements of the *IRAS* velocity covariance matrix $\langle \Delta u_i \Delta u_j \rangle$ into the space of the base functions F^j as described in DNW (eq. 21). In contrast to DNW, we argue here that the term, C_{LG} , describing the effect of an error in the LG motion, depends on β for the following reason. Both, the SFI and the *IRAS* fields suffer from errors resulting from the LG motion. Since only the difference $\alpha_{tf}^j - \alpha_{iras}^j$ enters in $\tilde{\chi}^2$ in (6), we must take into account any cancelation of the LG error in this difference. In the SFI velocities, this error amounts to a dipole term (filtered by the modal expansion). The effect in the *IRAS* velocities is slightly more complicated. An error in the LG motion, generates an artificial dipole component in the distribution of the *IRAS* galaxies in redshift space which, consequently, leads to a β dependent velocity dipole in the recovered *IRAS* velocity field. According to Nusser & Davis (1994) a dipole distribution generates a velocity dipole which, approximately, scales like $\beta/(1 + \beta)$. That implies that the residual error between the SFI and the *IRAS* field scales like $1/(1 + \beta)$. Therefore we write

$$C_{LG} = \frac{\sigma_{LG}^2}{(1 + \beta)^2} \cos(\theta_{ij}) \quad (9)$$

where θ_{ij} is the angle between the lines of sight to the points i and j and we set $\sigma_{LG} = 150 \text{ km s}^{-1}$ (see DNW).

We compute the Poisson error covariance matrix C_{SN} by generating 18 bootstrap realizations of the observed 1.2 Jy *IRAS* galaxy distribution by replacing each observed galaxy with a number of points drawn from a Poisson distribution with mean of unity. Then we compute the velocity fields from these realizations by the same algorithm used in the derivation of the velocity field from the observed galaxy distribution. For galaxy i of the SFI sample, we tabulate the differences, δu_i , between the velocity obtained from each of the 18 bootstrap realizations and the velocity as predicted from the actual distribution of galaxies, and evaluate the covariance matrix C_{SN} by averaging the product $\delta u_i \delta u_j$ from all the bootstrap realizations. This process is computed for several different values of β .

As in DNW, we model the non-linear term $C_{NL}(i, j)$ as

$$C_{NL}(i, j) = ((s_h(i) + s_h(j))^2 \exp\left(-\frac{|\Delta \mathbf{s}(i, j)|^2}{2\sigma_{coh}^2}\right)) \quad (10)$$

Where $\Delta \mathbf{s}(i, j)$ is the redshift separation between the galaxies i and j . We assume that the coherent error is proportional to the square of the average shear in the *IRAS* derived velocity fields for each β , $s_h \equiv \sigma_{NL} \min(1.67, |dv_p/dz|) \text{ km s}^{-1}$. We adopt a value of $\sigma_{coh} = 200 \text{ km s}^{-1}$. It is important to note that the amplitude, σ_{NL} , of this error is uncertain. Here, we choose $\sigma_{NL} = 90 \text{ km s}^{-1}$, which makes the value of the reduced $\tilde{\chi}^2$ unity at the minimum for $\sigma_\eta = 0.065$. The choice is natural based on the hypothesis that the SFI and *IRAS* fields independently describe the same underlying velocity field. Moreover the amplitude of the error is reasonable. However, we will compute $\tilde{\chi}^2(\beta)$ for various values of this error. Fortunately, the best β estimate is robust with respect to changes in the amplitude of this error.

Given the covariance matrices, we compute curves of the reduced $\tilde{\chi}^2(\beta)$, for the HR and LR filters. The results are summarized in figure 9, which shows curves of the reduced $\tilde{\chi}^2(\beta)$ for the two filters using various error estimates, as explained in the figure caption. For both filters, the minimum value of the $\tilde{\chi}^2$ is attained at $\beta = 0.6$ regardless of the details of our estimate of the covariance matrices. The 1-sigma error is less than 0.1 for all the curves. We have also computed curves of the reduced $\tilde{\chi}^2(\beta)$ for values of C_{LG} and C_{NL} not shown in figure 9 and find that the minimum is not sensitive to their exact values. The amplitude of C_{NL} was chosen so that the value of $\tilde{\chi}^2$ per degree of freedom for the LR filter is very close to unity when the nonlinear error is included. The corresponding value for the HR filter is 1.23, significantly larger than unity. This large value possibly indicates some disagreement between the fields on smaller scales. However, it is reassuring that the visual inspection of the fields reveals no gross discrepancies between them (figure 8). Note also that a large value of $\tilde{\chi}^2$ can be attributed to the fact that the scatter in the ITF relation is not strictly Gaussian, and since the effects of non-gaussianity are more important on small scales, we expect a larger deviation from a value of unity of the reduced $\tilde{\chi}^2$ for the HR filter. To evaluate the effect of the β dependence in the term C_{LG} , we computed $\tilde{\chi}^2$ using the expression of DNW which did not include the factor $1/(1 + \beta)$. Although the shape of the curve became flatter for $\beta > 0.6$ and steeper for smaller values of β , the minimum remained unchanged at $\beta = 0.6$.

It is interesting to inspect the correlation function of the residual fields. Figure 10 plots the correlation function of the quantity $P_{SFI} - P_{IRAS}$ for various values of β , where $P = -5 \log(1 - u/s)$ as defined in section 3. For comparison, the correlation function of P_{SFI} is also shown. The overall amplitude of the correlation function corresponding to the residual field for $\beta = 0.4$ or 0.6 is significantly smaller than that of the SFI field. Note that the curve corresponding to $\beta = 0.6$ which minimizes $\tilde{\chi}^2$ does not have the lowest amplitude at zero lag. The reason is clearly that the value of the correlation function at zero lag is simply the variance of the residual field and cannot be used to determine the best fit β as it does not include the covariance of the errors.

4.3 Comparison between the SFI and Mark III Results

As pointed out in the introduction, the ITF method has recently been applied to the Mark III catalog by DNW and their results can be used for an indirect assessment of the differences between the SFI and Mark III catalogs. DNW used 2900 spirals, in the Mark III catalog, including cluster and field galaxies. Notwithstanding the larger number of galaxies in the Mark III sample, the non-uniform sampling of the surveyed volume prevented DNW from carrying out the modal expansion with more than 56 modes of an effective resolution intermediate between our LR and HR fits.

Comparing our figure 3 with figure 8 of DNW we see that nearby the Mark III has considerably more points as it includes the Aarson et al. (1982) data. In the intermediated redshift shell the most significant difference is that the strong velocity gradient seen in the Mark III in the interval $240^\circ < l < 330^\circ$ and $15^\circ < b < 40^\circ$ is less pronounced in the SFI data. The flow there is predominantly determined by the MFB92 data which have been pruned to include only Sbc-Sc galaxies in the SFI (see section 2). In the SFI map there is an infall motion at $(210^\circ < l < 270^\circ, -40^\circ < b < -20^\circ)$ which is absent in the Mark III flow. This infall extends smoothly northward to the Great Attractor region. The most obvious differences between Mark III and SFI, not surprisingly, are seen in the last redshift shell. The general impression is that the dipole patterns in the two maps differ significantly in direction and amplitude. The direction of the dipole in the SFI map seems to lie along the direction of the reflex motion of the LG, while the Mark III dipole is directed along the south galactic pole. In sharp contrast to the SFI velocity field, the Mark III flow exhibits a strong infall in the northern cap. In the general direction of PP (lower left part of the slice), both SFI and Mark III flows have the same sign but with slightly different amplitudes. Note that the SFI galaxies cover that region more uniformly, illustrating the overall uniformity of the SFI.

5 SUMMARY AND DISCUSSION

The principal advantage of estimating β from velocity-velocity and density-density comparisons is that they are model independent. This is in contrast to other methods like the power spectrum analysis (Zaroubi et al. 1996) and redshift distortions (*e.g.*, Fisher et al. 1994, Hamilton 1993). Although the velocity-velocity and density-density comparisons are equivalent, in practice, they differ in several aspects. In particular velocity-velocity comparison on the basis of the modal expansion done here, requires no corrections to the biases which plague density-density comparisons. Moreover, nonlinear effects are less significant in the velocity-velocity comparison.

We have compared the observed SFI peculiar velocity field with that predicted from the galaxy distribution of the *IRAS* galaxies. We have found good agreement between the two fields for $\beta = 0.6 \pm 0.1$ with no dependence on depth. Similar values for β have been obtained by Freudling et al. (1997). We have determined β using filters with two different resolutions and found no evidence for scale dependence in the estimate of β . The good agreement between the fields is consistent with the galaxy distribution being closely related to that of the dark matter by means of a scale independent biasing factor, and with the hypothesis that the TF relation does not depend strongly on environment. It seems unreasonable that the biasing mechanism and the TF relation should conspire to yield such a good agreement between the fields.

Our estimate for β is consistent with the value determined by DNW from the comparison of the Mark III with the *IRAS* field. However, DNW found systematic discrepancies between the fields, which prevented a firm determination of β from their analysis. The major problem was the presence of a residual dipole component which strongly increased with depth beyond 3000 km s^{-1} . Our residual fields show no persisting coherent features in the comparison volume. That gives us confidence in our estimate for β and that the SFI flow field is a fair representation of the underlying velocity field.

The Mark III and the SFI flows seem exhibit some disagreement beyond a redshift of 3000 km s^{-1} . The differences between the flows at lower redshifts are not serious and can be understood in terms of the different selection criteria used in defining the two samples. Willick et al. (1997) presented a likelihood analysis of the *IRAS* and Mark III velocity fields within a distance of 3000 km s^{-1} . They found a good match between the Mark III and the *IRAS* fields in that limited volume and derived a value of $\beta \sim 0.5$. This is consistent with our estimate of β obtained from the analysis of the peculiar velocity field within 6000 km s^{-1} . This is another indication that the differences between the SFI and the Mark III catalog are to be found primarily at large distances. Resolving these discrepancies should allow us to combine the two samples in order to better constrain the local peculiar velocity field which is of great interest.

Estimates of β from velocity-velocity comparisons point towards values of β lower than obtained previously with different samples and other methods (*e.g.*, Dekel et al. 1993, Zaroubi et al. 1996). A value of $\beta = 0.6$ is consistent with other determinations obtained independently of large scale flows, *e.g.*, cluster abundance, galaxy power-spectrum and small-scale velocities. If the universe is flat, a value $\beta \sim 0.6$ requires a biasing factor of ~ 2 for optical galaxies. Such a high value for the biasing value implies a rather low normalization for the matter density fluctuations which is hard to reconcile with COBE-normalized CDM-like models. Moreover, such a large value for b is difficult to obtain in hierarchical structure formation (Kauffman, Nusser and Steinmetz 1997).

The results presented here are encouraging and demonstrate the importance of all-sky homogeneous measurements of peculiar velocities. Current samples are still too small and sparse to allow them to be used to explore smaller scales ($500 - 1500$

km s⁻¹) where non-linear effects become important. Future samples should aim at a higher sampling rate and uniform sky coverage.

ACKNOWLEDGEMENTS

We would like to thank Marc Davis for many valuable discussions and suggestions. The results presented in this paper are based on observations carried out at the National Astronomy and Ionosphere Center (NAIC), the National Radio Astronomy Observatory (NRAO), the Kitt Peak National Observatory (KPNO), the Cerro Tololo Interamerican Observatory (CTIO), European Southern Observatory, the Palomar Observatory (PO), the Observatory of Paris at Nançay and the Michigan–Dartmouth–MIT Observatory (MDM). NAIC, NRAO, KPNO and CTIO are respectively operated by Cornell University, Associated Universities, inc., and Associated Universities for Research in Astronomy, all under cooperative agreements with the National Science Foundation. Access to the 5m telescope at PO was guaranteed under an agreement between Cornell University and the California Institute of Technology. This research was supported by NSF grants AST94–20505 to RG, AST90-14850 and AST90-23450 to MH and AST93–47714 to GW who would also like to acknowledge support by ESO for a visit to Garching.

REFERENCES

- Aaronson, M., Huchra, J., Mould, J., Schechter, P. & Tully, R.B., 1982, *ApJ* 258, 64
 Carlberg, R.G., Yee, H.K.C., Ellingson, E., Abraham, R., Cravel, P., Morris, S. & Pritchett, C.J. 1996, *ApJ* 462, 32
 da Costa, L.N., Freudling, W., Wegner, G., Giovanelli, R., Haynes, M.P. & Salzer, J.J. 1996, *ApJ*, 468, L5
 Davis, M., Nusser, A. & Willick, J., 1996, *ApJ*, 473, 22 (DNW)
 Dekel, A., Bertschinger, E. Yahil, A., Strauss, M, Davis, M. & Huchra, J., 1993, *ApJ* 412, 1
 Fisher, K. B. , Davis, M., Strauss, M., Yahil, A. & Huchra, J., 1994, *MNRAS* 267, 927
 Fisher, K.B., Lahav, O., Hoffman, Y., Lynden-Bell, D. & Zaroubi, S., 1995, *MNRAS* 272, 885
 Freudling, W., da Costa, L.N., Giovanelli, R., Haynes, M.P., Salzer, J.J. & Wegner 1997, *in preparation*
 Giovanelli, R., Haynes, M.P., Herter, T., Vogt, N., Salzer, J.J., Wegner, G., da Costa, L.N. & Freudling, W. 1997a, *AJ* 113, 22
 Giovanelli, R., Haynes, M.P., Herter, T., Vogt, N., da Costa, L.N., Freudling, W. Salzer, J.J. & Wegner, G., 1997b, *AJ* 113, 53
 Hamilton, A.J.S. 1993, *ApJ*, 406, 247
 Haynes et al. 1997, *in preparation*
 Kauffman, G., Nusser, A. & Steinmetz, M. , 1997, *MNRAS* 286, 795
 Kochanek, C.S., 1996, *ApJ*, 466, 638
 Mathewson, D.S., Ford, V.L. and Buchhorn, M. 1992, *ApJS* 81, 413 (MFB92)
 Nusser, A. & Davis, M., 1994, *ApJ*, 421, L1
 Nusser, A. & Davis, M., 1995, *ApJ*, 449, 439 (ND95)
 Perlmutter et al., 1997, *ApJ* 483, 565
 Persic, M. and Salucci, P. 1995, *ApJS* 99, 501
 Schechter, P. 1980, *ApJ* 85, 801
 Willick, J.A., Courteau, S., Faber S.M., Burstein, D., Dekel, A. and Strauss, M. A. 1997, *ApJS* 109, 333
 Willick, J.A., Strauss, M.A., Dekel, A & Kollat, T., 1997, *preprint*
 Zaroubi, S., Zehavi, I., Dekel, A. & Kollat, T. 1997, *ApJ. in press*

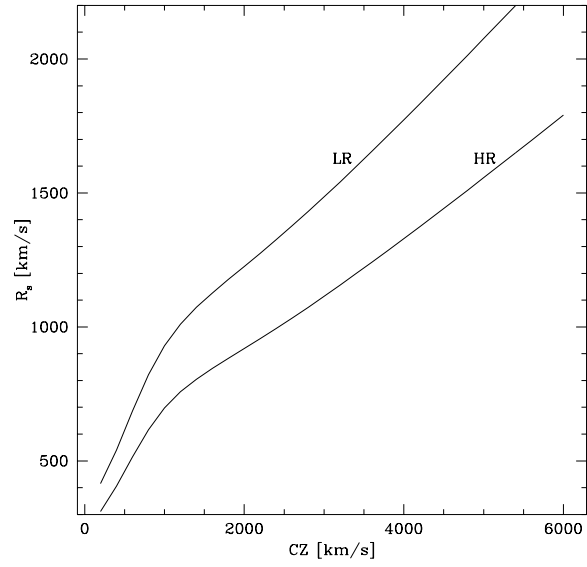


Figure 1. The radial resolution scale of the filters HR and LR as a function of redshift. At any redshift, the smoothing of the filters roughly corresponds to a sharp cutoff of $k_s = 2\pi/R_s$ in k-space.

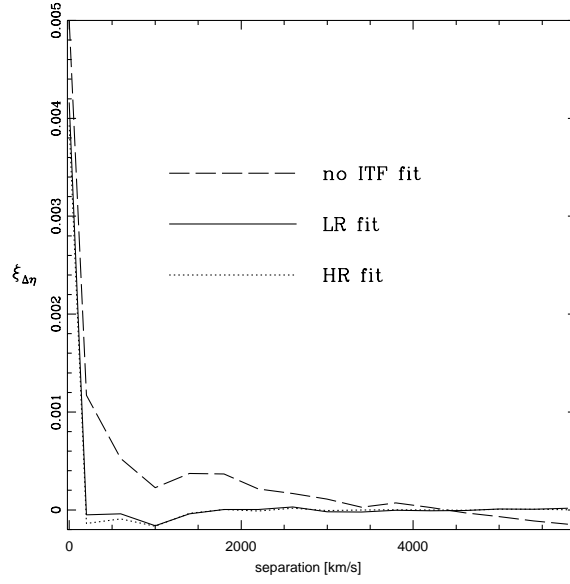


Figure 2. The autocorrelation function of the η residuals of the SFI galaxies versus redshift space separation. The dashed curve is before the ITF fitting, while the solid and dotted are after the ITF fitting with the LR and HR respectively.

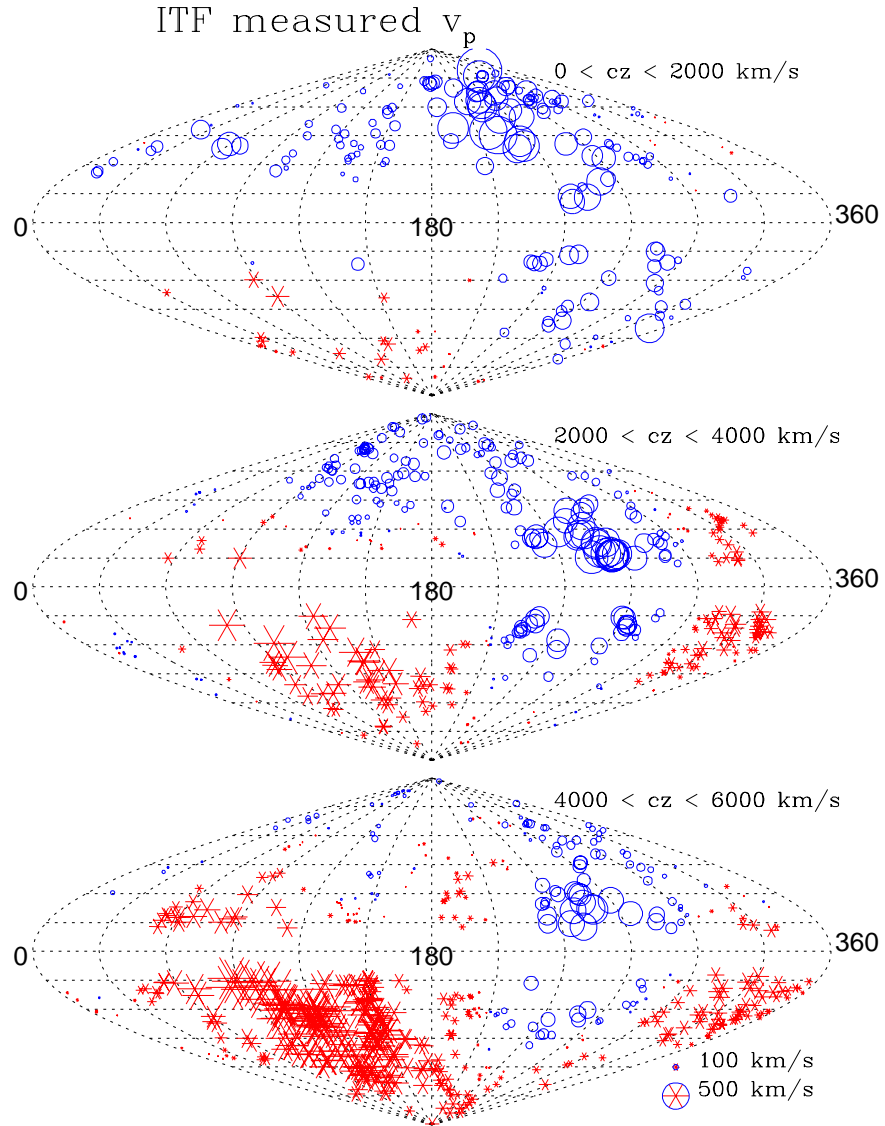


Figure 3. The sky projection in galactic coordinates as seen in the LG frame of the low resolution ITF velocity field for the SFI galaxies

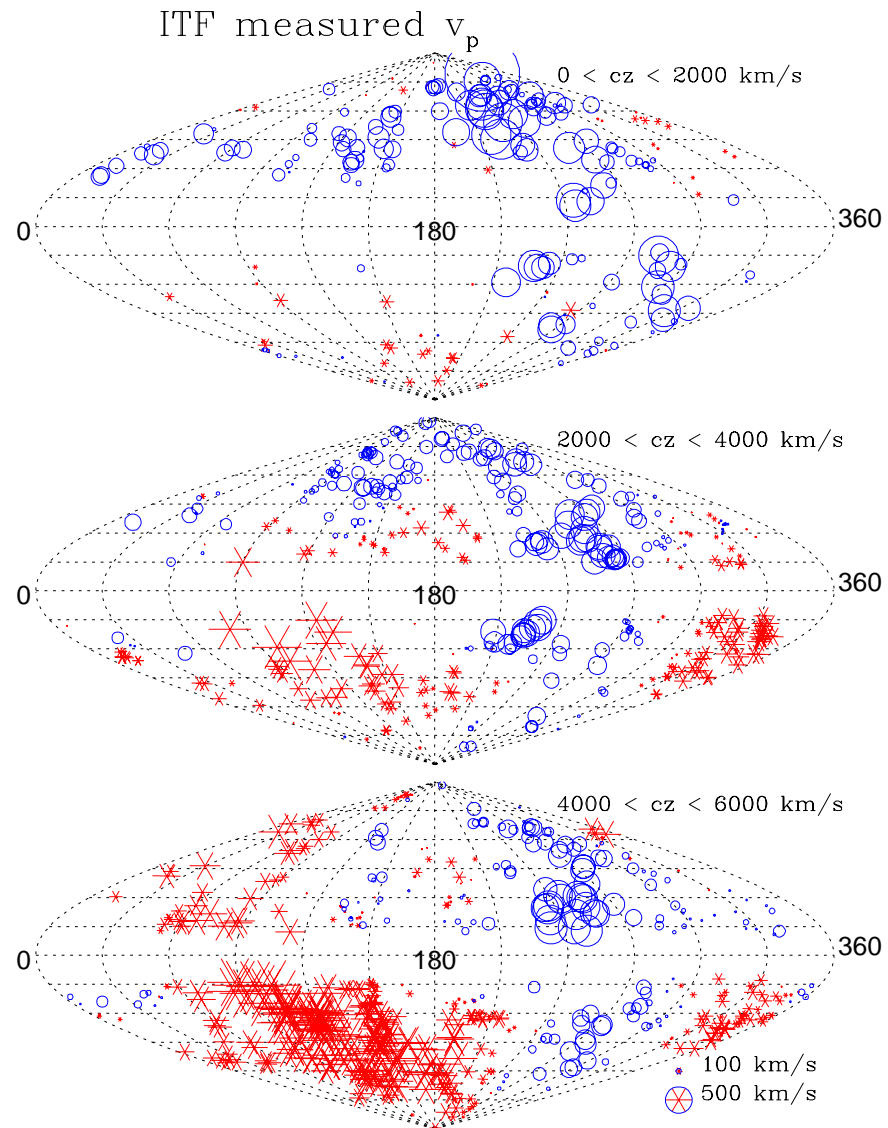


Figure 4. The high resolution ITF velocity field for the SFI galaxies using the same sky projection as figure 3

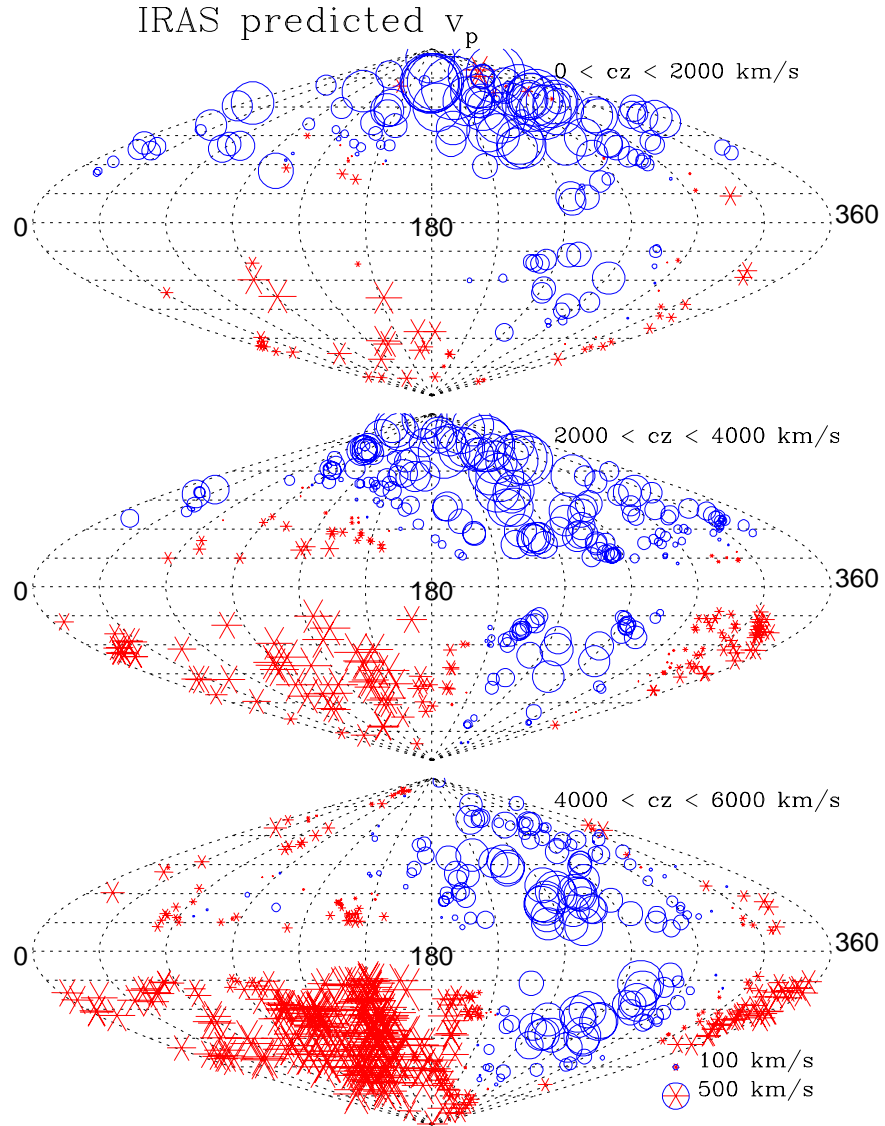


Figure 5. The low resolution velocity field for the *IRAS* galaxies for $\beta = 1$

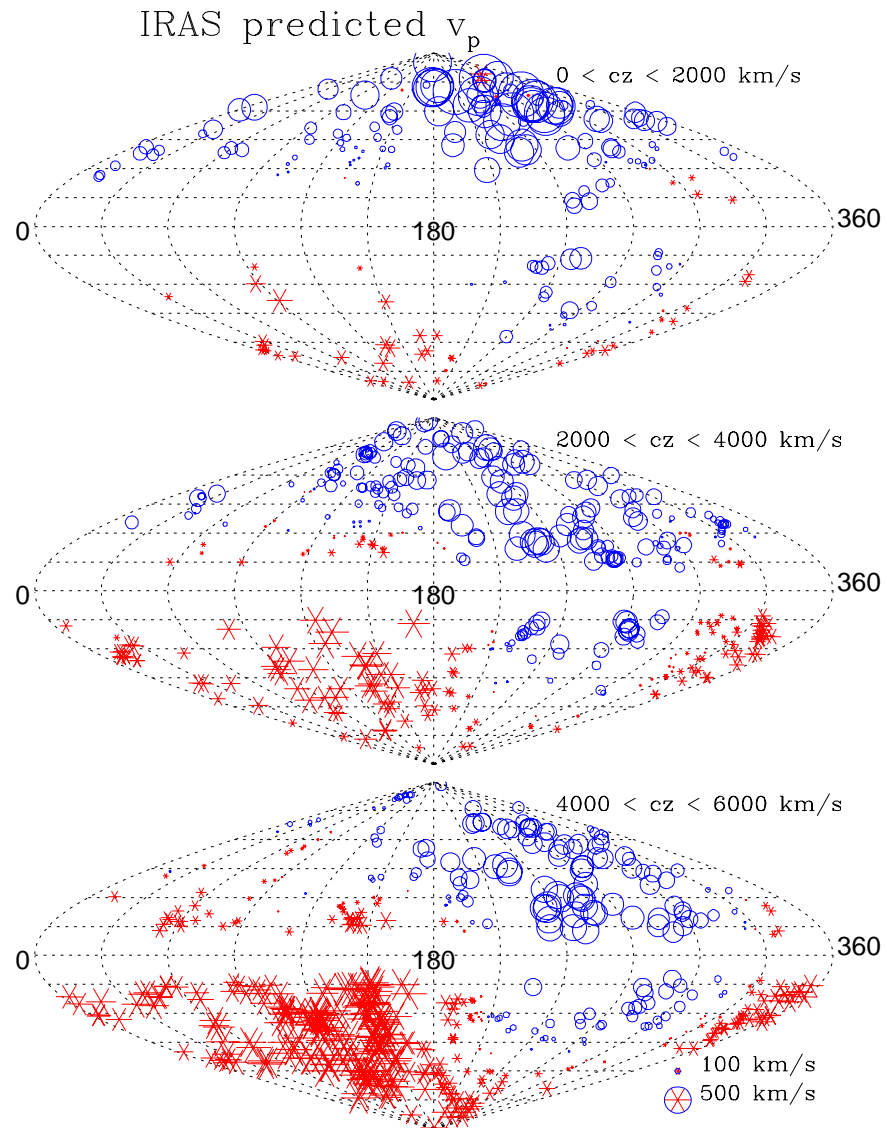


Figure 6. The low resolution velocity field for the *IRAS* galaxies for $\beta = 0.6$

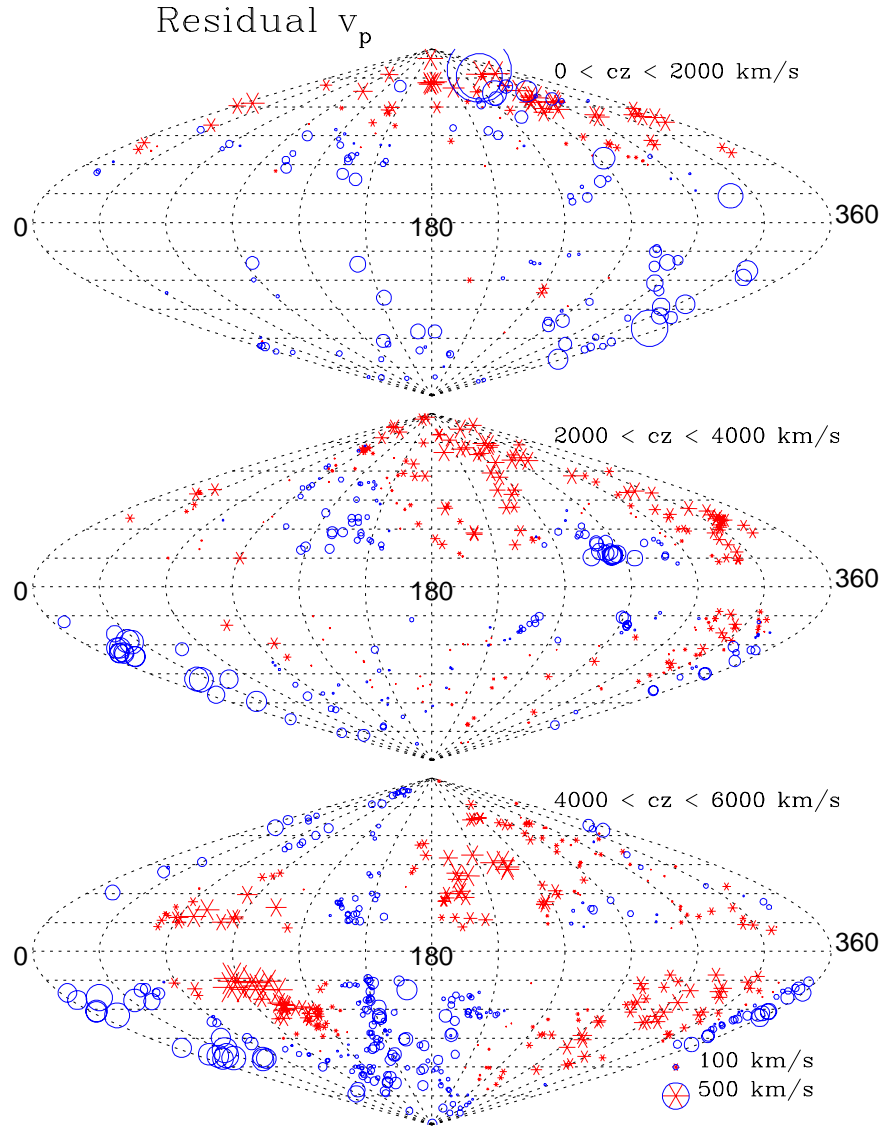


Figure 7. The sky projection of the residuals $u_{SFI} - u_{IRAS}$ for $\beta = 0.6$, for low resolution fits

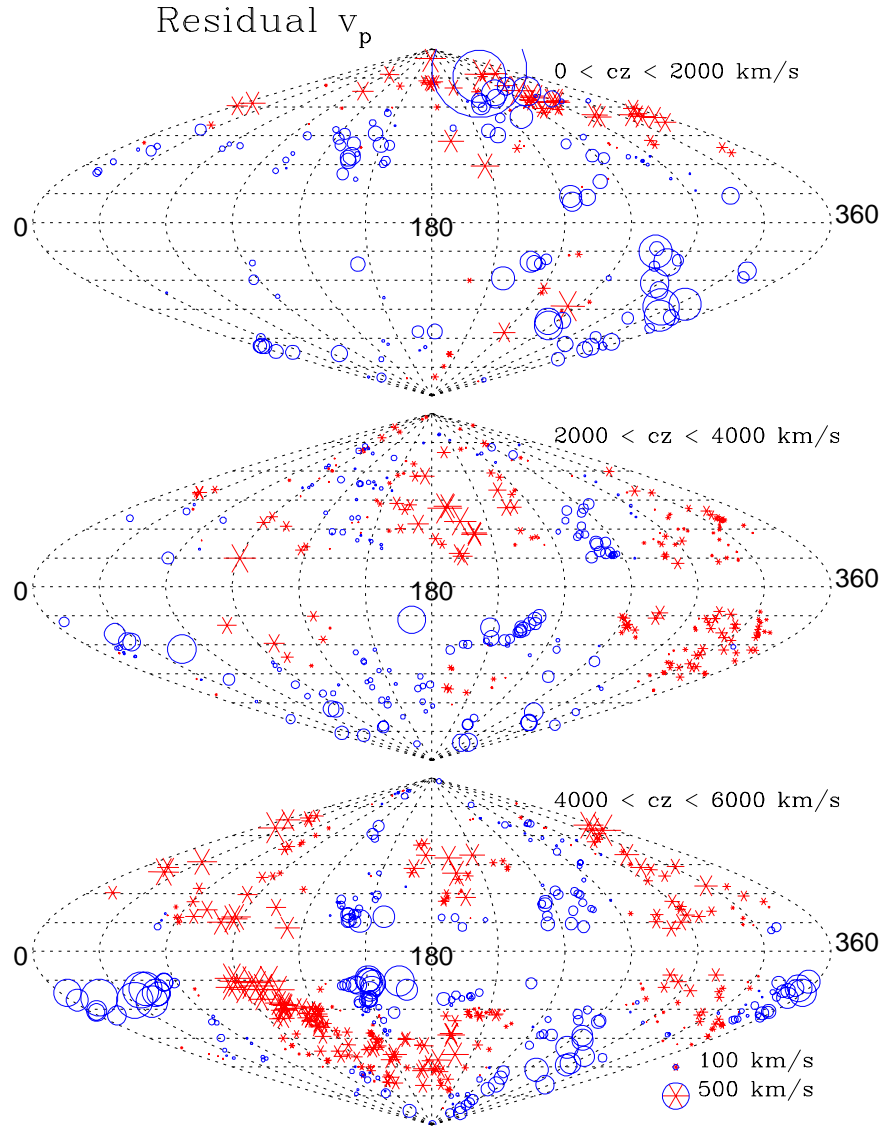


Figure 8. The sky projection of the residuals $u_{SFI} - u_{IRAS}$ for $\beta = 0.6$, for the high resolution fits

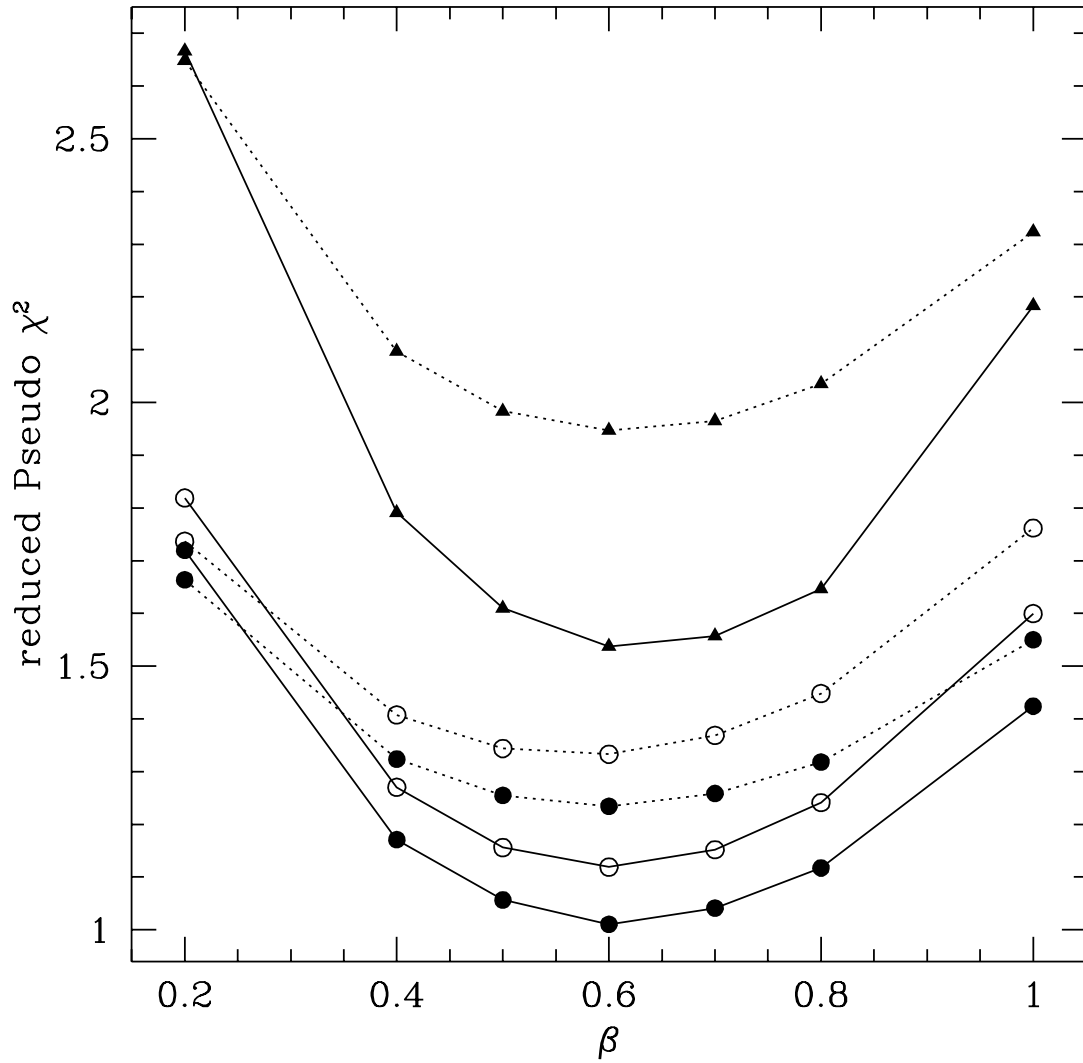


Figure 9. Curves of reduced Pseudo- χ^2 versus β computed using equation (6) for the LR (solid lines) and HR (dotted lines), filters. Shown are curves for two different values for $\sigma_\eta = 0.065$ (circles) and 0.05 (triangles), with (filled symbols) or without (open symbols) the non-linear error C_{NL} .

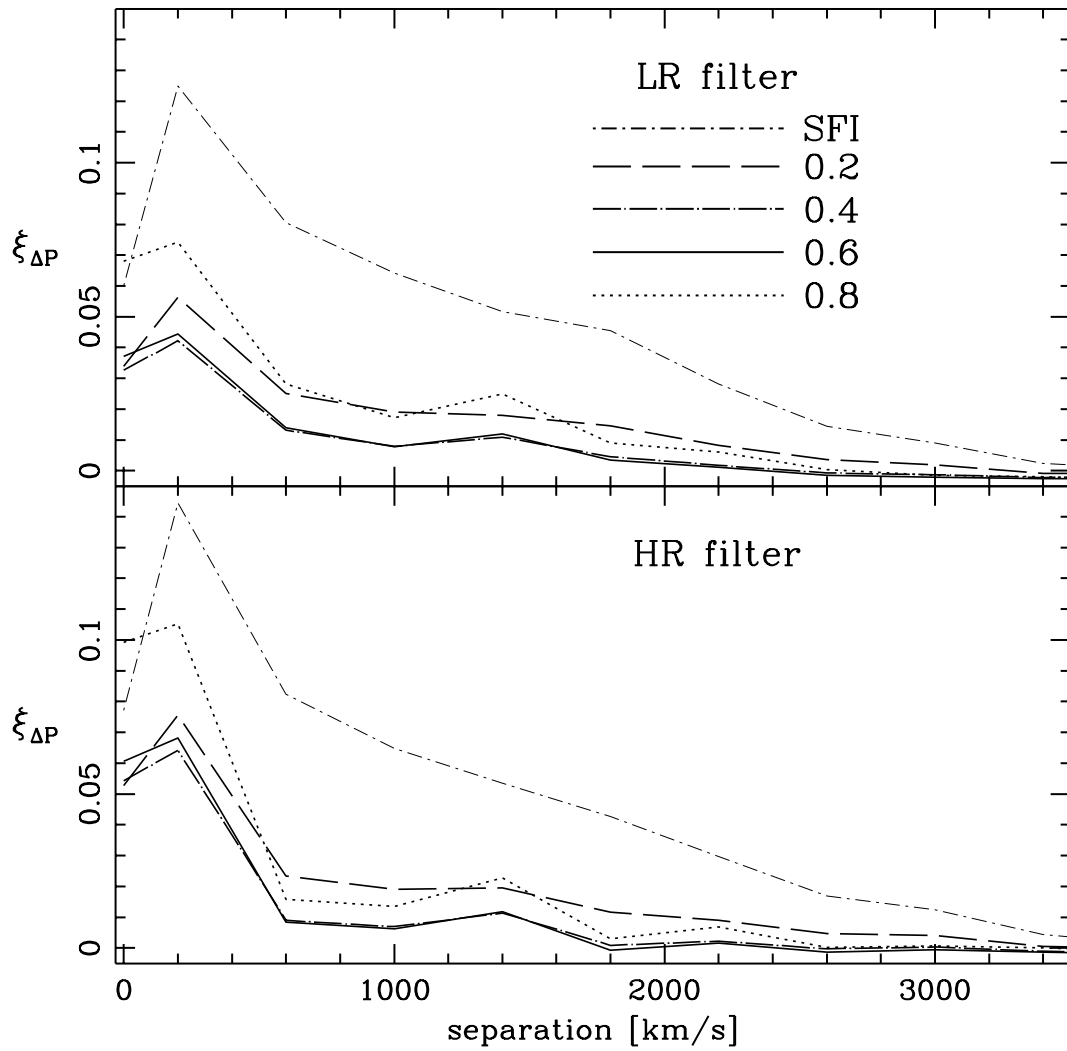


Figure 10. The correlations function of $\Delta P = P_{SFI} - P_{IRAS}$ for various values of β as indicated in the plot. For comparison we also show the correlation function of the SFI field